Coupled Systems Mechanics, *Vol. 8, No. 1 (2019) 1-17*
DOI: https://doi.org/10.12989/csm.2019.8.1.001

Influence of sine material gradients on delamination in multilayered beams

Victor I. Rizov*

Department of Technical Mechanics, University of Architecture, Civil Engineering and Geodesy, 1 Chr. Smirnensky Blvd., 1046 – Sofia, Bulgaria

(Received February 12, 2018, Revised June 11, 2018, Accepted December 7, 2018)

Abstract. The present paper deals with delamination fracture analyses of the multilayered functionally graded non-linear elastic Symmetric Split Beam (SSB) configurations. The material is functionally graded in both width and height directions in each layer. It is assumed that the material properties are distributed non-symmetrically with respect to the centroidal axes of the beam cross-section. Sine laws are used to describe the continuous variation of the material properties in the cross-sections of the layers. The delamination fracture is analyzed in terms of the strain energy release rate by considering the balance of the energy. A comparison with the J-integral is performed for verification. The solution derived is used for parametric analyses of the delamination fracture behavior of the multilayered functionally graded SSB in order to evaluate the effects of the sine gradients of the three material properties in the width and height directions of the layers and the location of the crack along the beam width on the strain energy release rate. The solution obtained is valid for two-dimensional functionally graded non-linear elastic SSB configurations which are made of an arbitrary number of lengthwise vertical layers. A delamination crack is located arbitrary between layers. Thus, the two crack arms have different widths. Besides, the layers have individual widths and material properties.

Keywords: multilayered beam; delamination fracture; material non-linearity; two-dimensional sine material gradient

1. Introduction

Functionally graded materials are a promising alternative to homogeneous structural materials mainly because by gradual varying the material properties along one or more spatial directions during manufacturing, one can get optimum performance of functionally graded structural members and components to external loads (Bensaid and Kerboua 2017, Bensaid *et al.* 2017, Bohidar *et al.* 2014, Gasik 2010, Hirai and Chen 1999, Koizumi 1993, Markworth *et al.* 1995, Mortensen and Suresh 1995, Nemat-Allal *et al.* 2011, Neubrand and Rödel 1997, Uslu Uysal and Kremzer 2015, Uslu Uysal 2016, Uslu Uysal and Güven 2016, Uslu Uysal 2017). In structural applications of functionally graded materials, facture is a critical failure mode. The inhomogeneous character of functionally graded materials imposes a significant difficulty in

*Corresponding author, Professor, E-mail: V_RIZOV_FHE@UACG.BG

http://www.techno-press.org/?journal=csm&subpage=8 ISSN: 2234-2184 (Print), 2234-2192 (Online)

fracture analyses of functionally graded structures.

Multilayered materials are manufactured by bonding of layers of different materials. Recently, multilayered materials have been used as advanced structural materials in various engineering applications (Markov and Dinev 2005). One of the major drawbacks of the layered materials is their high susceptibility to delamination fracture (Dolgov 2005, 2016). Delamination, i.e., separation of layers, considerably reduces the strength and stiffness of multilayered structural members and components and even may lead to catastrophic failure (Guadette *et al.* 2001, Narin 2006, Hsueh *et al.* 2009, Szekrenyes 2010, Szekrenyes 2016a, b).

An interesting work on delamination fracture behavior of multilayered beam configurations has been published by Narin (2006). The analysis has been carried-out by assuming linear-elastic mechanical behavior of the material in each layer. Thus, the principles of linear-elastic fracture mechanics have been applied. The delamination has been studied in terms of the strain energy release rate. Methods for analyzing the strain energy release rate have been developed with considering the influence of residual stresses. The effect of temperature differences on the delamination fracture behavior has also been analyzed and discussed. Delamination behavior of several multilayered beam configurations has been investigated.

Delamination fracture in multilayered linear-elastic beam configurations subjected to four-point bending has been analyzed by Hsueh *et al.* (2009). A solution to the strain energy release rate has been obtained by applying methods of linear-elastic fracture mechanics. The solution can be used for multilayered four-point bending beam systems with any number of layers. It is assumed that the delamination cracking can occur at any interface.

Delamination fracture in multilayered functionally graded beam structures has been analyzed recently also with considering the non-linear behaviour of the material by Rizov (2017a), (2017b), (2017c), Rizov (2018). The material non-linearity has been described by a power-law stress-strain relation. By considering the complementary strain energy, analytical solutions for the strain energy release rate have been derived assuming that only one material property (the coefficient of the power law stress-strain relation) is functionally graded.

The purpose of the present paper is to develop a delamination fracture analysis of the multilayered functionally graded non-linear elastic SSB configuration assuming that the material is functionally graded in both width and height directions of each layer. The three material properties, which are involved in the non-linear stress-strain relation, vary continuously in the cross-section of each layer according to a sine law (the properties are distributed non-symmetrically with respect to the centroidal axes of the beam cross-section). The solution for the strain energy release rate, derived by analyzing the balance of the energy, is applied to evaluate the influences of sine material gradients along the width and height of the layers, the delamination crack location along the beam width and the non-linear mechanical behavior of the functionally graded material on the delamination fracture.

2. Analysis of the strain energy release rate

The multilayered functionally graded SSB configuration that is analyzed in the present paper is shown schematically in Fig. 1. The beam is made of lengthwise vertical layers. Perfect adhesion is assumed between the layers. The number of the layers is arbitrary. Also, the layers have different widths and material properties. Besides, the functionally graded material in each layer exhibits non-linear mechanical behaviour. The beam cross-section is a rectangle of width, b, and height, h.

The beam length is 2*l*. A notch of depth, b_2, is introduced in the right-hand lateral surface of the beam in order to generate conditions for delamination fracture. A delamination crack is located symmetrically with respect to the beam mid-span. The crack length is 2*a*. The delamination crack is located arbitrary along the beam width. The widths of the left-hand and the right-hand crack arms are denoted by b_1 and b_2, respectively. The boundaries of the left-hand crack arm are $l-a \le x_3 \le l+a$, $-b/2 \le y_3 \le b_1 - b/2$ and $-h/2 \le z_3 \le h/2$. The right-hand crack arm has the following boundaries: $l-a \le x_3 \le l+a$, $b_1 - b/2 \le y_3 \le b/2$ and $-h/2 \le z_3 \le h/2$.

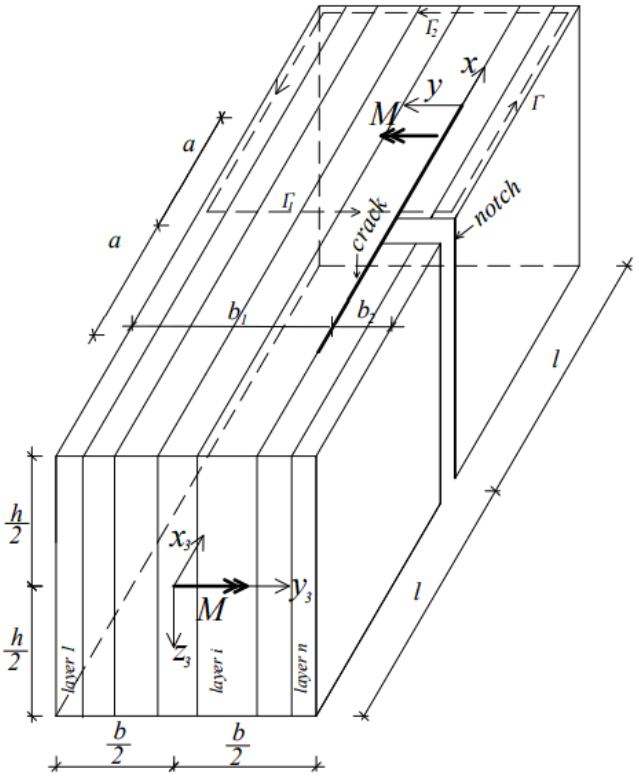

Fig. 1 The geometry of the multilayered functionally graded SSB configuration

The notch divides the right-hand crack arm in two symmetric segments of length, *a*, each. The beam is loaded by two moments, *M*, applied at the end sections of the beam (Fig. 1). Obviously, the two segments of the right-hand crack arm are free of stresses. It should be noted that the normal stresses induced by the bending of the SSB configuration around the horizontal centroidal axis of the beam cross-section generate a combination between mode two and mode three cracking.

Due to the symmetry, only half of the beam, $l \le x_3 \le 2l$, is analyzed (Fig. 1).

The delamination fracture is studied in terms of the strain energy release rate, *G*, by analyzing

the balance of the energy. By assuming an increase of the crack length, δa, the balance of the energy is written as

$$M\delta\varphi = \frac{\partial U}{\partial a}\delta a + Gh\delta a\,, \tag{1}$$

where $\delta\varphi$ is the increase of the rotation of the end section of the beam, U is the strain energy cumulated in half of the beam. Form (1), one arrives at

$$G = \frac{M}{h}\frac{\partial\varphi}{\partial a} - \frac{1}{h}\frac{\partial U}{\partial a}\,. \tag{2}$$

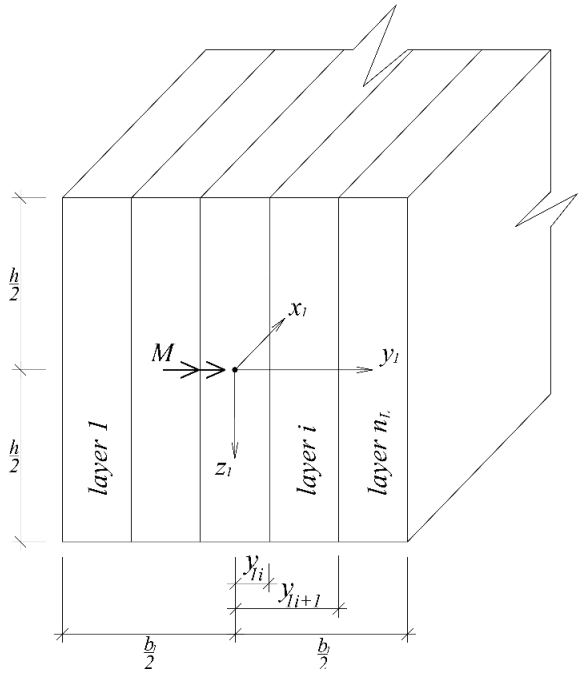

Fig. 2 The cross-section of the left-hand crack arm in the beam mid-span

It should be mentioned that the present analysis is performed assuming validity of the small strains hypothesis. Besides, the present analysis holds for non-linear elastic behaviour of the material. However, the analysis is applicable also for elastic-plastic behaviour if the beam under consideration undergoes active deformation, i.e., if the external loading increases only (Chakrabarty 2006, Lubliner 2006).

The rotation of the end section of the beam, φ, is determined by the Castigliano's theorem for structures exhibiting material non-linearity

$$\varphi = \frac{\partial U^*}{\partial M}\,, \tag{3}$$

where U^* is the complementary strain energy cumulated in half of the beam.

Since the two segments of the right-hand crack arm are free of stresses (Fig. 1), the complementary strain energy cumulated in half of the beam is written as

$$U^* = U_L^* + U_U^*, \tag{4}$$

where U_L^* and U_U^* are the complementary strain energies cumulated, respectively, in the left-hand crack arm and the un-cracked beam portion, $l + a \le x_3 \le 2l$.

By addition of the complementary strain energies cumulated in the layers of the left-hand crack arm, U_L^* is expressed as

$$U_L^* = a \sum_{i=1}^{i=n_L} \int_{y_{1i}}^{y_{1i+1}} \int_{-\frac{h}{2}}^{\frac{h}{2}} u_{0L_i}^* dy_1 dz_1, \tag{5}$$

where n_L is the number of the layers in the left-hand crack arm, y_{1i} and y_{1i+1} are the coordinates, respectively, of the left-hand and the right-hand lateral surfaces of the i-th layer (Fig. 2), $u_{0L_i}^*$ is the complementary strain energy density in the same layer, y_1 and z_1 are the centroidal axes of the cross-section of the left-hand crack arm.

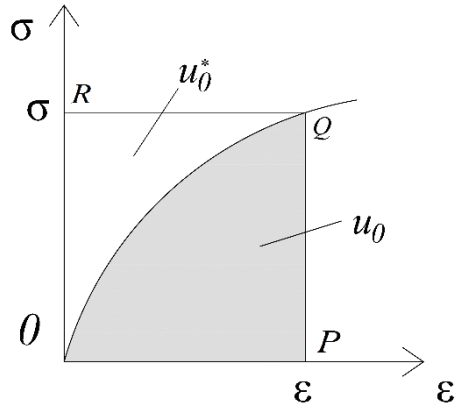

Fig. 3 Schematic of a non-linear stress-strain curve (the strain energy and the complementary strain energy densities are denoted by u_0 and u_0^*, respectively)

In principle, the complementary strain energy density is equal to the area, *OQR*, which supplements the area, *OPQ*, enclosed by the stress-strain curve to a rectangle (Fig. 3). Thus, $u_{0L_i}^*$ is written as

$$u_{0L_i}^* = \sigma_i \varepsilon - u_{0L_i}, \tag{6}$$

where σ_i is the distribution of the longitudinal normal stresses in the i-th layer of the left-hand crack arm, ε is the distribution of the longitudinal strains, u_{0Li} is the strain energy density in the same layer. The strain energy density is equal to the area, OPQ, enclosed by the stress-strain curve (Fig. 3). Therefore, u_{0Li} is expressed as

$$u_{0L_i} = \int_0^{\varepsilon} \sigma_i d\varepsilon \,. \tag{7}$$

In the present paper, the non-linear mechanical behaviour of the functionally graded material in the i-th layer is described by the following stress-strain relation (Lukash 1998)

$$\sigma_i = E_i \left[1 - \left(1 - \frac{\varepsilon}{\beta_i} \right)^{r_i} \right], \tag{8}$$

where E_i, β_i and r_i are material properties.

By combining of (7) and (8), one obtains

$$u_{0L_i} = E_i \varepsilon + \frac{E_i \beta_i}{r_i + 1} \left(1 - \frac{\varepsilon}{\beta_i} \right)^{r_i + 1} - \frac{E_i \beta_i}{r_i + 1} \,. \tag{9}$$

From (6), (8) and (9), one derives

$$u^*_{0L_i} = -E_i \varepsilon \left(1 - \frac{\varepsilon}{\beta_i} \right)^{r_i} - \frac{E_i \beta_i}{r_i + 1} \left(1 - \frac{\varepsilon}{\beta_i} \right)^{r_i + 1} + \frac{E_i \beta_i}{r_i + 1} \,. \tag{10}$$

It assumed that the material properties, E_i, β_i and r_i, which are involved in the stress-strain relation (8), are functionally graded in both width and height directions in each layer. The continuous variation of E_i, β_i and r_i in the cross-section of the i-th layer is described by the following sine laws

$$E_i = E_{0_i} \left[1 + f_{E_i} \sin \left(\frac{y_1 - y_{1i}}{y_{1i+1} - y_{1i}} \frac{\pi}{2} \right) + g_{E_i} \sin \left(\frac{z_1 + \frac{h}{2}}{h} \frac{\pi}{2} \right) \right], \tag{11}$$

$$\beta_i = \beta_{0_i} \left[1 + f_{\beta_i} \sin \left(\frac{y_1 - y_{1i}}{y_{1i+1} - y_{1i}} \frac{\pi}{2} \right) + g_{\beta_i} \sin \left(\frac{z_1 + \frac{h}{2}}{h} \frac{\pi}{2} \right) \right], \tag{12}$$

$$r_i = r_{0_i} \left[1 + f_{r_i} \sin \left(\frac{y_1 - y_{1i}}{y_{1i+1} - y_{1i}} \frac{\pi}{2} \right) + g_{r_i} \sin \left(\frac{z_1 + \frac{h}{2}}{h} \frac{\pi}{2} \right) \right], \tag{13}$$

where f_{E_i}, f_{β_i} and f_{r_i} are material properties which govern the material gradients, respectively,

of E_i, β_i and r_i along y_1 axis. The material gradients of E_i, β_i and r_i along z_1 axis are governed by g_{E_i}, g_{β_i} and g_{r_i}, respectively. Formulae (11), (12) and (13) indicate that E_i, β_i and r_i are distributed non-symmetrically with respect to y_1 and z_1. It should be noted that the sine laws provide smooth material gradients in both width and height directions in each layer.

The distribution of the longitudinal strains is analyzed assuming validity of the Bernoulli's hypothesis for plane sections, since the span to height ratio of the beam under consideration is large. It should also be noted that since the beam is loaded in pure bending, the only non-zero strain is ε. Thus, according to the small strains compatibility equations, ε is distributed linearly in the cross-section. Hence, the strain distribution in the cross-section of the left-hand crack arm is written as

$$\varepsilon = \varepsilon_{C_1} + \kappa_{y_1} y_1 + \kappa_{z_1} z_1, \tag{14}$$

where ε_{C_1} is the strain in the centre of the cross-section, κ_{y_1} and κ_{z_1} are the curvatures of left-hand crack arm in the x_1y_1 and x_1z_1 planes, respectively.

The following equations for equilibrium of the cross-section of the left-hand crack arm are used to determine ε_{C_1}, κ_{y_1} and κ_{z_1}

$$N_1 = \sum_{i=1}^{i=n_L} \int_{y_{1i}}^{y_{1i+1}} \int_{-\frac{h}{2}}^{\frac{h}{2}} \sigma_i dy_1 dz_1 , \tag{15}$$

$$M_{y_1} = \sum_{i=1}^{i=n_L} \int_{y_{1i}}^{y_{1i+1}} \int_{-\frac{h}{2}}^{\frac{h}{2}} \sigma_i z_1 dy_1 dz_1 , \tag{16}$$

$$M_{z_1} = \sum_{i=1}^{i=n_L} \int_{y_{1i}}^{y_{1i+1}} \int_{-\frac{h}{2}}^{\frac{h}{2}} \sigma_i y_1 dy_1 dz_1 , \tag{17}$$

where N_1 is the axial force, M_{y_1} and M_{z_1} are the bending moments about y_1 and z_1 axes, respectively. It is obvious that (Fig. 2)

$$N_1 = 0, \; M_{y_1} = M , \; M_{z_1} = 0 . \tag{18}$$

By substituting of (8), (11), (12), (13) and (14) in (15), (16) and (17), one derives

$$N_1 = h \sum_{i=1}^{i=n_L} E_{0_i} \left(\chi_i c_i + \frac{1}{2} q_i \upsilon_i + \frac{1}{3} \nu_i \phi_i \vartheta_i \right), \tag{19}$$

$$M_{y_1} = \frac{h^3}{12}\sum_{i=1}^{i=n_L} E_{0_i}\left[\left(\mu_i\lambda_i + \zeta_i\eta_i\right)\chi_i + \frac{1}{2}\left(\nu_i\lambda_i + \zeta_i\phi_i\right)\upsilon_i\right], \tag{20}$$

$$M_{z_1} = h\sum_{i=1}^{i=n_L} E_{0_i}\left[\frac{1}{2}\upsilon_i c_i + \frac{1}{3}q_i\vartheta_i + \frac{1}{4}\nu_i\phi_i\left(y_{1i+1}^4 - y_{1i}^4\right)\right], \tag{21}$$

where

$$\psi_i = \frac{\pi}{2\left(y_{1i+1} - y_{1i}\right)}, \tag{22}$$

$$\gamma_i = -y_{1i}\pi\,, \tag{23}$$

$$\delta = \frac{\pi}{2h}, \tag{24}$$

$$\theta_i = \beta_{0_i}\left(1 + f_{\beta_i}\sin\gamma_i + g_{\beta_i}0.707\right), \tag{25}$$

$$\omega_i = 1 - \frac{\varepsilon_{C_1}}{\theta_i}, \tag{26}$$

$$\varphi_i = r_{0_i}\left(1 + f_{r_i}\sin\gamma_i + g_{r_i}0.707\right), \tag{27}$$

$$\phi_i = \omega_i^{\varphi_i}\left(\frac{\varphi_i}{\omega_i}\frac{\kappa_{y_1}\theta_i - \varepsilon_{C_1}\beta_{0_i}f_{\beta_i}\psi_i\cos\gamma_i}{\theta_i^2} - r_{0_i}f_{r_i}\psi_i\cos\gamma_i\,\lg\omega_i\right), \tag{28}$$

$$\lambda_i = \omega_i^{\varphi_i}\left(\frac{\varphi_i}{\omega_i}\frac{\kappa_{z_1}\theta_i - \varepsilon_{C_1}\beta_{0_i}g_{\beta_i}\delta 0.707}{\theta_i^2} - r_{0_i}g_{r_i}\delta 0.707\,\lg\omega_i\right), \tag{29}$$

$$\chi_i = y_{1i+1} - y_{1i}\,, \tag{30}$$

$$\upsilon_i = y_{1i+1}^2 - y_{1i}^2\,, \tag{31}$$

$$\vartheta_i = y_{1i+1}^3 - y_{1i}^3\,, \tag{32}$$

$$\mu_i = 1 + f_{E_i}\sin\gamma_i + 0.707g_{E_i}\,, \tag{33}$$

$$\nu_i = f_{E_i}\psi_i\cos\gamma_i\,, \tag{34}$$

$$\zeta_i = 0.707 g_{E_i} \delta \,, \tag{35}$$

$$c_i = \mu_i \eta_i + \zeta_i \lambda_i \frac{h^2}{12} \,, \tag{36}$$

$$q_i = \mu_i \phi_i + \nu_i \eta_i \ . \tag{37}$$

It should be noted that at $n_L = 1$, $f_{E_i} = 0$, $g_{E_i} = 0$, $f_{\beta_i} = 0$, $g_{\beta_i} = 0$, $f_{r_i} = 0$ and $g_{r_i} = 1$, formulae (19), (20) and (21) transform in

$$N_1 = E_{0_i} \varepsilon_{C_1} bh \,, \tag{38}$$

$$M_{y_1} = E_{0_i} \frac{bh^3}{12} \kappa_{z_1} \,, \tag{39}$$

$$M_{z_1} = E_{0_i} \frac{b^3 h}{12} \kappa_{y_1} \,. \tag{40}$$

The fact that (38), (39) and (40) are exact matches of the equations for equilibrium of linear-elastic homogeneous beam of rectangular cross-section of width, b_1, and height, h, indicates the consistency of Eqs. (19), (20) and (21) since at β_i=1 and r_i=1 the non-linear stress-strain relation (8) transforms into the Hooke's law assuming that E_{0_i} is the modulus of elasticity.

Eqs. (19), (20) and (21) should be solved with respect to ε_{C_1}, κ_{y_1} and κ_{z_1} by using the MatLab computer program.

The complementary strain energy cumulated in the un-cracked beam portion is written as

$$U_U^* = (l-a) \sum_{i=1}^{i=n} \int_{y_{2i}}^{y_{2i+1}} \int_{-\frac{h}{2}}^{\frac{h}{2}} u_{0U_i}^* dy_2 dz_2 \,, \tag{41}$$

where n is the number of the layers, y_{2i} and y_{2i+1} are the coordinates, respectively, of the left-hand and the right-hand lateral surfaces of the i-th layer, $u_{0U_i}^*$ is the complementary strain energy density in the same layer, y_2 and z_2 are the centroidal axes of the beam cross-section.

Formula (10) is applied to obtain $u_{0U_i}^*$. For this purpose, E_i, β_i, r_i and ε are replaced with E_{U_i}, β_{U_i}, r_{U_i} and ε_U, respectively (E_{U_i}, β_{U_i} and r_{U_i} are the distributions of the material properties in the i-th layer of the un-cracked beam portion, ε_U is the distribution of the longitudinal strains in the un-cracked beam portion). Formulae (11), (12), (13) and (14) are used to obtain E_{U_i}, β_{U_i}, r_{U_i} and ε_U, respectively. For this purpose, y_1, y_{1i}, y_{1i+1}, z_1, ε_{C_1}, κ_{y_1} and κ_{z_1} are replaced with y_2, y_{2i},

y_{2i+1}, z_2, ε_{C_2}, κ_{y_2} and κ_{z_2}, respectively (ε_{C_2} is the strain in the centre of the cross-section of the un-cracked beam portion, κ_{y_2} and κ_{z_2} are the curvatures of the un-cracked beam portion in x_2y_2 and x_2z_2 planes, respectively). Equilibrium Eqs. (19), (20) and (21) are used to determine ε_{C_2}, κ_{y_2} and κ_{z_2}. For this purpose, N_1, M_{y_1}, M_{z_1}, n_L, ε_{C_1}, κ_{y_1}, κ_{z_1}, y_{1i}, y_{1i+1}, ψ_i, γ_i, θ_i, ω_i, φ_i, ϕ_i, λ_i, χ_i, υ_i, ϑ_i, μ_i, μ_i, ζ_i, c_i and q_i are replaced, respectively, with N_2, M_{y_2}, M_{z_2}, n, ε_{C_2}, κ_{y_2}, κ_{z_2}, y_{2i}, y_{2i+1}, ψ_{U_i}, γ_{U_i}, θ_{U_i}, ω_{U_i}, φ_{U_i}, ϕ_{U_i}, λ_{U_i}, χ_{U_i}, υ_{U_i}, ϑ_{U_i}, μ_{U_i}, μ_{U_i}, ζ_{U_i}, c_{U_i} and q_{U_i} in formulae (19)-(37), where N_2 is the axial force in the un-cracked beam portion, M_{y_2} and M_{z_2} are the bending moments about y_2 and z_2 axes (apparently, N_2=0, M_{y2}=M and M_{z2}=0).

The strain energy in half of the beam is written as

$$U = U_L + U_U, \tag{42}$$

where U_L and U_u are the strain energies cumulated in the left-hand crack arm and the un-cracked beam portion, respectively.

The strain energy in the left-hand crack arm is expressed as

$$U_L = a\sum_{i=1}^{i=n_L}\int_{y_{1i}}^{y_{1i+1}}\int_{-\frac{h}{2}}^{\frac{h}{2}} u_{0L_i}\,dy_1dz_1, \tag{43}$$

where the strain energy density, u_{0Li}, in the i-th layer of the left-hand crack arm is obtained by (9).

The strain energy cumulated in the un-cracked beam portion is written as

$$U_U = (l-a)\sum_{i=1}^{i=n}\int_{y_{2i}}^{y_{2i+1}}\int_{-\frac{h}{2}}^{\frac{h}{2}} u_{0U_i}\,dy_2dz_2, \tag{44}$$

where u_{0U_i} is determined by (9). For this purpose, E_i, β_i, r_i and ε are replaced with E_{U_i}, β_{U_i}, r_{U_i} and ε_U, respectively.

The expression obtained by substituting of (3), (4), (5), (41), (42), (43) and (44) in (2) is doubled in view of the symmetry (Fig. 1). In this manner, one arrives at

$$\begin{aligned} G = 2\Bigg[& \frac{M}{h}\frac{\partial}{\partial M}\left(\sum_{i=1}^{i=n_L}\int_{y_{1i}}^{y_{1i+1}}\int_{-\frac{h}{2}}^{\frac{h}{2}} u_{0L_i}^{*}\,dy_1dz_1 - \sum_{i=1}^{i=n}\int_{y_{2i}}^{y_{2i+1}}\int_{-\frac{h}{2}}^{\frac{h}{2}} u_{0U_i}^{*}\,dy_2dz_2\right) - \\ & -\frac{1}{h}\left(\sum_{i=1}^{i=n_L}\int_{y_{1i}}^{y_{1i+1}}\int_{-\frac{h}{2}}^{\frac{h}{2}} u_{0L_i}\,dy_1dz_1 - \sum_{i=1}^{i=n}\int_{y_{2i}}^{y_{2i+1}}\int_{-\frac{h}{2}}^{\frac{h}{2}} u_{0U_i}\,dy_2dz_2\right)\Bigg]. \end{aligned} \tag{45}$$

The integration in (45) should be performed by the MatLab computer program. The derivative,

$\frac{\partial}{\partial M}(...)$, in (45) should be determined numerically by the MatLab computer program.

The strain energy release rate (45) is verified by the *J*-integral approach (Rice 1968, Broek 1986). The integration is carried-out along the integration contour, Γ, shown by a dashed line in Fig. 1. It is obvious that the *J*-integral has non-zero values only in segments, Γ_1 and Γ_2, of the integration contour, where Γ_1 coincides with the cross-section of the left-hand crack arm in the beam mid-span, Γ_2 coincides with the end section of the beam (Fig. 1). Therefore, the *J*-integral is obtained as

$$J = J_{\Gamma_1} + J_{\Gamma_2}\,, \tag{46}$$

where J_{Γ_1} and J_{Γ_2} are the values of the integral in segments Γ_1 and Γ_2, respectively.

The *J*-integral in segment, Γ_1, is written as

$$J_{\Gamma_1} = \sum_{i=1}^{i=n_L} \int_{y_{1i}}^{y_{1i+1}} \left[u_{0L_i} \cos\alpha - \left(p_{xi} \frac{\partial u}{\partial x} + p_{yi} \frac{\partial v}{\partial x} \right) \right] ds\,, \tag{47}$$

where α is the angle between the outwards normal vector to the contour of integration and the crack direction, p_{xi} and p_{yi} are the components of stress vector in the *i*-th layer of the left-hand crack arm, u and v are the components of displacement vector with respect to the coordinate system xy (x is directed along the delamination crack), ds is a differential element along the contour.

The components of J_{Γ_1} are determined as

$$p_{xi} = -\sigma_i\,, \tag{48}$$

$$p_{yi} = 0\,, \tag{49}$$

$$ds = dy_1\,, \tag{50}$$

$$\cos\alpha = -1, \tag{51}$$

where σ_i is expressed as a function of ε by (8). The following formula from Mechanics of materials is applied to obtain the partial derivative, $\partial u/\partial x$, in (47)

$$\frac{\partial u}{\partial x} = \varepsilon = \varepsilon_{C_1} + \kappa_{y_1} y_1 + \kappa_{z_1} z_1\,. \tag{52}$$

The *J*-integral in segment, Γ_2, is expressed as

$$J_{\Gamma_2} = \sum_{i=1}^{i=n} \int_{y_{2i}}^{y_{2i+1}} \left[u_{0U_i} \cos\alpha_U - \left(p_{xU_i} \frac{\partial u}{\partial x_U} + p_{yU_i} \frac{\partial v}{\partial x_U} \right) \right] ds_U\,, \tag{53}$$

where

$$p_{xU_i} = \sigma_i\,, \tag{54}$$

$$p_{yU_i} = 0\,, \tag{55}$$

$$ds_U = -dy_2\,, \tag{56}$$

$$\cos\alpha_U = 1, \tag{57}$$

$$\frac{\partial u}{\partial x_U} = \varepsilon_{C_2} + \kappa_{y_2} y_2 + \kappa_{z_2} z_2\,. \tag{58}$$

The stress, σ_i, in (54) is obtained by (8). For this purpose, E_i, β_i, r_i and ε are replaced with E_{U_i}, β_{U_i}, r_{U_i} and ε_U, respectively.

The average value of the J-integral along the delamination crack front is written as

$$J_{av} = \frac{1}{h}\int_{-\frac{h}{2}}^{\frac{h}{2}} J\,dz_1\,. \tag{59}$$

By substituting of (46), (47) and (53) in (59) and doubling of the expression obtained in view of the symmetry (Fig. 1), one arrives at

$$\begin{aligned} J_{av} = {} & \frac{2}{h}\sum_{i=1}^{i=n_L}\int_{-\frac{h}{2}}^{\frac{h}{2}}\int_{y_{1i}}^{y_{1i+1}}\left[u_{0L_i}\cos\alpha - \left(p_{xi}\frac{\partial u}{\partial x} + p_{yi}\frac{\partial v}{\partial x}\right)\right]ds\,dz_1 + \\ & + \frac{2}{h}\sum_{i=1}^{i=n}\int_{-\frac{h}{2}}^{\frac{h}{2}}\int_{y_{2i}}^{y_{2i+1}}\left[u_{0U_i}\cos\alpha_U - \left(p_{xU_i}\frac{\partial u}{\partial x_U} + p_{yU_i}\frac{\partial v}{\partial x_U}\right)\right]ds_U\,dz_1\,. \end{aligned} \tag{60}$$

The MatLab computer program should be used to perform the integration in (60). It should be noted that the J-integral values obtained by (60) match the strain energy release rates found by (45). This fact is a verification of the delamination fracture analysis of the multilayered functionally graded SSB configuration developed in the present paper.

3. Parametric analysis

A parametric analysis of the delamination fracture in the multilayered functionally graded SSB configuration is performed. Two three-layered functionally graded beams are investigated (Fig. 4). A delamination crack is located between layers 2 and 3 in the beam shown in Fig. 4(a). A beam with a delamination between layers 1 and 2 is also analyzed (Fig. 4(b)). The width of each layer is t (Fig. 4). The external loading consists of two moments, M, applied at the ends of the beams. It is

assumed that t=0.003 m, h=0.014 m and M=40 Nm. The influence of the material gradients of E_i, β_i and r_i in both width and height directions of layer 1 on the delamination fracture behaviour are investigated.

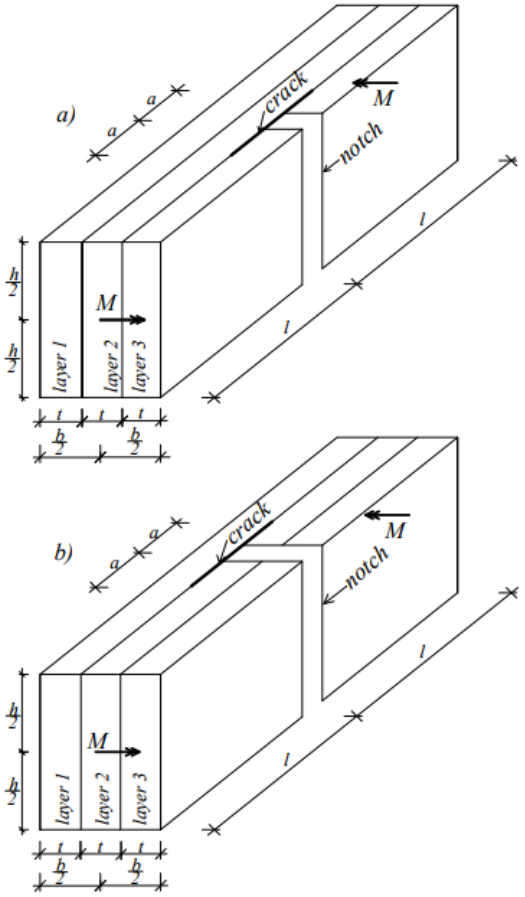

Fig. 4 Two three-layered functionally graded SSB configurations

For this purpose, calculations of the strain energy release rate are carried-out by applying formula (45). The strain energy release rate is presented in non-dimensional form by using the formula, $G_N = G/(E_{0_1} h)$. The effect of material property, f_{E_1}, on the strain energy release rate for both three-layered SSB configurations (Fig. 4) is illustrated in Fig. 5. It is assumed that $f_{E_2} = 0.8$, $f_{E_3} = 1.2$, $g_{E_1} = 0.6$, $g_{E_2} = 0.9$, $g_{E_3} = 1.1$, $E_{0_2}/E_{0_1} = 0.8$, $E_{0_3}/E_{0_1} = 1.6$, $f_{\beta_1} = 0.4$, $f_{\beta_2} = 0.2$, $f_{\beta_3} = 0.5$, $g_{\beta_1} = 0.3$, $g_{\beta_2} = 0.4$, $g_{\beta_3} = 0.6$, $\beta_{0_1} = 0.3$, $\beta_{0_2} = 0.6$, $\beta_{0_3} = 0.4$, $f_{r_1} = 0.1$, $f_{r_2} = 0.3$, $f_{r_3} = 0.2$, $g_{r_1} = 0.2$, $g_{r_2} = 0.1$, $g_{r_3} = 0.3$, $r_{0_1} = 0.4$, $r_{0_2} = 0.1$ and $r_{0_3} = 0.5$.

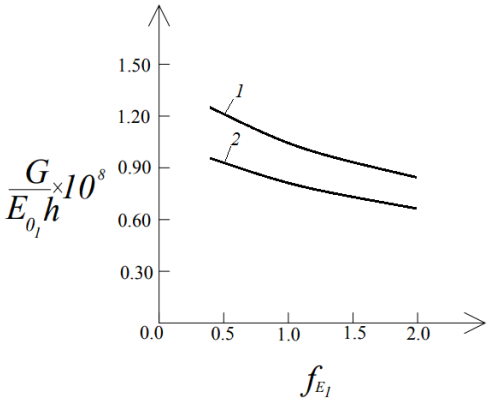

Fig. 5 The strain energy release rate in non-dimensional form plotted against f_{E_1} for a delamination crack located between layers 2 and 3 (curve 1) and for a delamination crack located between layers 1 and 2 (curve 2)

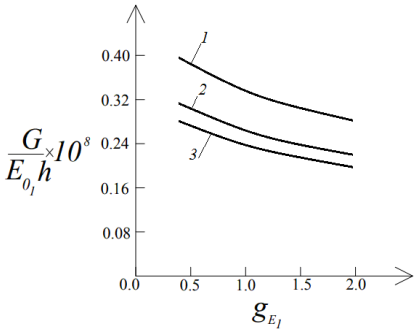

Fig. 6 The strain energy release rate in non-dimensional form plotted against g_{E_1} at non-linear behaviour of the functionally graded material (curve 1) and linear-elastic behaviour of the functionally graded material (curve 2) for the three-layered SSB configuration shown in Fig. 4(a)

The curves in Fig. 5 indicate that the strain energy release rate decreases with increasing of f_{E_1}. This finding is attributed to the fact that the beam stiffness increases when f_{E_1} increases. One can observe also in Fig. 5 that the strain energy release rate increases when the crack location is changed from this shown in Fig. 4(a) to that in Fig. 4(b). This behaviour is due to the decrease of the left-hand crack arm stiffness.

The influence of material property, g_{E_1}, on the fracture behaviour is evaluated too. The beam configuration shown in Fig. 4(a) is analyzed. The strain energy release rate in non-dimensional form is plotted in against g_{E_1} Fig. 6. It can be observed in Fig. 6 that the strain energy release rate decreases with increasing of g_{E_1}. The effect of the non-linear mechanical behaviour of the functionally graded material on the strain energy release rate is also illustrated in Fig. 6. For this purpose, the strain energy release rate obtained assuming linear-elastic behaviour of the functionally graded material is plotted in non-dimensional form in Fig. 6 for comparison with the non-linear solution. It should be mentioned that the linear-elastic solution for the strain energy

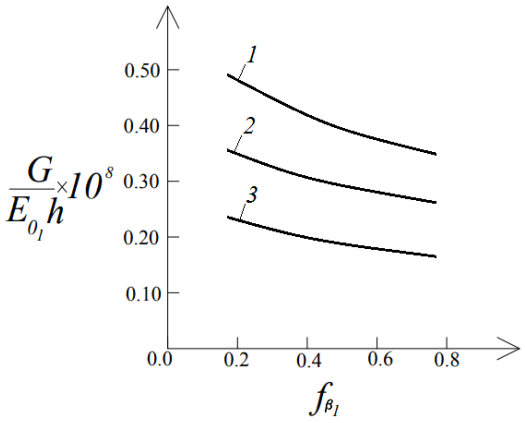

Fig. 7 The strain energy release rate in non-dimensional form plotted against f_{β_1} at $g_{\beta_1}=0.2$ (curve 1), $g_{\beta_1}=0.4$ (curve 2) and $g_{\beta_1}=0.6$ (curve 3) for the three-layered SSB configuration shown in Fig. 4(a)

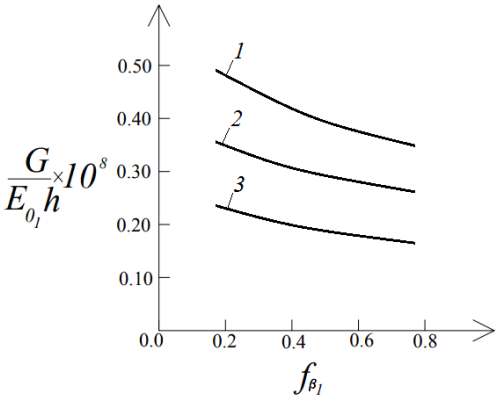

Fig. 8 The strain energy release rate in non-dimensional form plotted against f_{r_1} at $g_{r_1}=0.1$ (curve 1), $g_{r_1}=0.2$ (curve 2) and $g_{r_1}=0.3$ (curve 3) for the three-layered SSB configuration shown in Fig. 4(a)

release rate is derived by substituting of $\beta_{0_i}=1$, $f_{\beta_i}=0$, $g_{\beta_i}=0$, $r_{0_i}=1$, $f_{r_i}=0$ and $g_{r_i}=0$ in (45). One can observe in Fig. 6 that the material non-linearity leads to increase of the strain energy release rate.

The influence of material properties, f_{β_1} and g_{β_1}, on the strain energy release rate in the three-layered functionally graded SSB configuration shown in Fig. 4(a) is also explored. The strain energy release rate in non-dimensional form is presented as a function of f_{β_1} in Fig. 7 at three values of g_{β_1}. The diagrams in Fig. 7 show that the strain energy release rate decreases with increasing of f_{β_1} and g_{β_1}.

The effects of material properties, f_{r_1} and g_{r_1}, on the delamination fracture behaviour are also

evaluated. The SSB configuration shown in Fig. 4(a) is analyzed. The strain energy release rate in non-dimensional form is plotted against f_{r_1} in Fig. 8 at three values of g_{r_1}. It can be observed in Fig. 8 that the strain energy release rate decreases with increasing of f_{r_1} and g_{r_1}.

4. Conclusions

Analyses of the delamination fracture in the multilayered functionally graded SSB configurations which exhibit non-linear mechanical behaviour of the material are developed. The SSB is made of an arbitrary number of adhesively bonded lengthwise vertical layers which have individual widths and material properties.

The non-linear mechanical behaviour of the material in each layer is described by a non-linear stress-strain relation that involves three material properties.

It is assumed that the three material properties are functionally graded in both width and height directions in each layer. Sine laws are used to describe the continuous variations of the material properties in the layers (the material properties are distributed non-symmetric with respect to the centroidal axes of the beam cross-section). Fracture is studied in terms of the strain energy release rate by analyzing the balance of the energy. The solution derived is compared with the *J*-integral for verification. The effects of gradients of the material properties along the width and height of the layers on the delamination fracture are investigated. The influence of delamination crack location along the width of the beam cross-section is analyzed too. The main findings of the present delamination fracture study can be summarized as follows:

- The strain energy release rate decreases with increasing of f_{E_1} and g_{E_1}.
- The increase of f_{β_1} and g_{β_1} leads to decrease of the strain energy release rate.
- The strain energy release rate decreases with increasing of f_{r_1} and g_{r_1}.
- The strain energy release rate decreases when the width of the cross-section of the left-hand crack arm increases.

References

Bensaid, I. and Kerboua, B. (2017), "Interfacial stress analysis of functionally graded beams strengthened with a bonded hydrothermal aged composite panel", *Compos. Interf.*, **24**(2), 149-169.

Bensaid, I., Cheikh, A., Mangouchi, A. and Kerboua, B. (2017), "Static deflection and dynamic behaviour of higher-order hyperbolic shear deformable compositionally graded beams", *Adv. Mater. Res.*, **6**(1), 13-26.

Bohidar, S.K., Sharma, R. and Mishra, P.R. (2014), "Functionally graded materials: A critical review", *Int. J. Res.*, **1**(7), 289-301.

Broek, D. (1986), *Elementary Engineering Fracture Mechanics*, Springer.

Chakrabarty, J. (2006), *Theory of Plasticity*, Elsevier Butterworth-Heinemann, Oxford.

Dolgov, N.A. (2005), "Determination of stresses in a two-layer coating", *Strength Mater.*, **37**(4), 422-431.

Dolgov, N.A. (2016), "Analytical methods to determine the stress state in the substrate-coating system under mechanical loads", *Strength Mater.*, **48**(5), 658-667.

Gasik, M.M. (2010), "Functionally graded materials: Bulk processing techniques", *Int. J. Mater. Prod. Technol.*, **39**(1-2), 20-29.

Guadette, F.G., Giannapoulos, A.E. and Suresh, S. (2001), "Interfacial cracks in layered materials subjected

to a uniform temperature change", *Int. J. Fract.*, **28**, 5620-5629.
Hirai, T. and Chen, L. (1999), "Recent and prospective development of functionally graded materials in Japan", *Mater. Sci. For.*, **308-311**(4), 509-514.
Hsueh, C.H., Tuan, W.H. and Wei, W.C.J. (2009), "Analyses of steady-state interface fracture of elastic multilayered beams under four-point bending", *Script. Mater.*, **60**(8), 721-724.
Koizumi, M. (1993), "The concept of FGM ceramic trans", *Function. Grad. Mater.*, **34**(1), 3-10.
Lubliner, J. (2006), *Plasticity Theory (Revised Edition)*, University of California, Berkeley, California, U.S.A.
Lukash, P.A. (1998), *Fundamentals of Non-Linear Structural Mechanics*, Stroizdat.
Markov, I. and Dinev, D. (2005), "Theoretical and experimental investigation of a beam strengthened by bonded composite strip", *Reports of International Scientific Conference VSU'2005*, 61-68.
Markworth, A.J., Ramesh, K.S. and Parks, Jr.W.P. (1995), "Review: Modeling studies applied to functionally graded materials", *J. Mater. Sci.*, **30**(3), 2183-2193.
Mortensen, A. and Suresh, S. (1995), "Functionally graded metals and metal-ceramic composites: Part 1 processing", *Int. Mater. Rev.*, **40**(6), 239-265.
Narin, J.A. (2006), "On the calculation of energy release rates for cracked laminates with residual stresses", *Int. J. Fract.*, **139**(2), 267-293.
Nemat-Allal, M.M., Ata, M.H., Bayoumi, M.R. and Khair-Eldeen, W. (2011), "Powder metallurgical fabrication and microstructural investigations of aluminum/steel functionally graded material", *Mater. Sci. Appl.*, **2**(5), 1708-1718.
Neubrand, A. and Rödel, J. (1997), "Gradient materials: An overview of a novel concept", *Zeit. f. Met.*, **88**(4), 358-371.
Rice, J.R. (1968), "A path independent integral and the approximate analysis of strain concentrations by notches and cracks", *J. Appl. Mech.*, **35**(2), 379-386.
Rizov, V.I. (2017a), "Non-linear analysis of delamination fracture in functionally graded beams", *Coupled Syst. Mech.*, **6**(1), 97-111.
Rizov, V.I. (2017b), "Non-linear elastic delamination of multilayered functionally graded beam", *Multidiscipl. Model. Mater. Struct.*, **13**(4), 434-447.
Rizov, V.I. (2017c), "Delamination of multilayered functionally graded beams with material nonlinearity", *Int. J. Struct. Stab. Dyn.*, **18**(4), 1850051.
Rizov, V.I. (2018), "Non-linear fracture analysis of multilayered two-dimensional graded beams", *Multidiscipl. Model. Mater. Struct.*, **14**(2), 387-399.
Szekrenyes, A. (2010), "Fracture analysis in the modified split-cantilever beam using the classical theories of strength of materials", *J. Phys.: Conf. Ser.*, **240**, 012030.
Szekrenyes, A. (2016a), "Semi-layerwise analysis of laminated plates with nonsingular delamination-the theorem of autocontinuity", *Appl. Math. Model.*, **40**(2), 1344-1371.
Szekrenyes, A. (2016b), "Nonsingular crack modelling in orthotropic plates by four equivalent single layers", *Eur. J. Mech.-A/Sol.*, **55**, 73-99.
Uslu Uysal, M. (2017), "Virtual crack closure technique on delamination fracture toughness of composite materials based on epoxy resin filled with micro-scale hard coal", *Acta Phys. Polonic. A*, In Press.
Uslu Uysal, M. and Güven, U. (2016), "A bonded plate having orthotropic inclusion in adhesive layer under in-plane shear loading", *J. Adhes.*, **92**(3), 214-235.
Uslu Uysal, M. and Kremzer, M. (2015), "Buckling behaviour of short cylindrical functionally gradient polymeric materials", *Acta Phys. Polonic. A*, **127**(4), 1355-1357.
Uysal, M. (2016), "Buckling behaviours of functionally graded polymeric thin-walled hemispherical shells", *Steel Compos. Struct.*, **21**(4), 849-862.